Towards an Interferometric Autofocus for the Estimation of Ionospheric Signatures in Biomass

Betancourt-Payan, Felipe[a], Rodriguez-Cassola, Marc[a], Prats-Iraola, Pau[a], and Krieger, Gerhard[a]
[a]Deutsches Zentrum fuer Luft- und Raumfahrt (DLR), Muenchener Str. 20, 82234 Wessling, Germany

Abstract

This paper presents the workflow towards an improved estimation and correction of phase errors due to trans-ionospheric propagation in low-frequency Synthetic Aperture Radar (SAR) images when interferometric stacks are available. The method consists of estimating the absolute ionospheric phase delays in each of the images with traditional methods like autofocus. These setimations will later be combined with what is obtained during the correction of the differential ionosphere in interferometric pairs. By running the algorithms on simulated data, it is shown that it is possible to resolve faster changing phase errors than with the autofocus alone for a more accurate correction.

1 Introduction

The use of lower frequencies in Synthetic Aperture Radar (SAR) is motivated by the penetration capability of the radar waves into volumetric scatterers like forests and ice. The achieved lower temporal decorrelation is also desired in the processing of interferometric products and motivated the development of new systems like the P-band SAR Biomass (435 MHz) [1]. These low-frequency radio waves are also significantly affected by the double passage through the ionosphere [2, 3], which leaves a footprint in the images that must be corrected to improve the quality and interpretation of the data. On the other hand, since to calibrate the ionosphere effects, we first need to *see it*, it also offers the potential of high resolution 2D ionospheric imaging [4].

The refractive index experienced by the radar waves changes with the concentration of free electrons and frequency. In the presence of the ionosphere, the lower the frequency, the larger the phase errors introduced into the SAR images [5]. The phase errors that occur due to small ionospheric irregularities are particularly interesting. They produce defocussing in the azimuth dimension, lowering the contrast and resolution of the images. In the interferograms, this irregular part of the ionosphere introduces azimuth shifts between the image pairs and phase screens. For the imaging and calibration of ionospheric effects in the Biomass framework, there are different approaches, based on the estimation of the Faraday rotation [6], one Map-Drift Autofocus (MDA) [7, 8] or the combination of both [9]. In this paper, we will focus on using the MDA calibration only. There are also different methods for the correction of phase errors in the interferograms, such as range split-spectrum, azimuth shifts, or a combination of both too [10].

In this paper, we present a method that attempts to regain resolution in the estimation of the single-pass solutions by using the results obtained by the interferometric calibration. These last estimations have higher resolutions, and the combination is possible via a system of linear transformations. Section 2 explains the methodology, Section 3 describes the scenario used for the simulations carried out and that lead to the results in Section 4. Section 5 presents a summary and conclusions.

2 Methodology

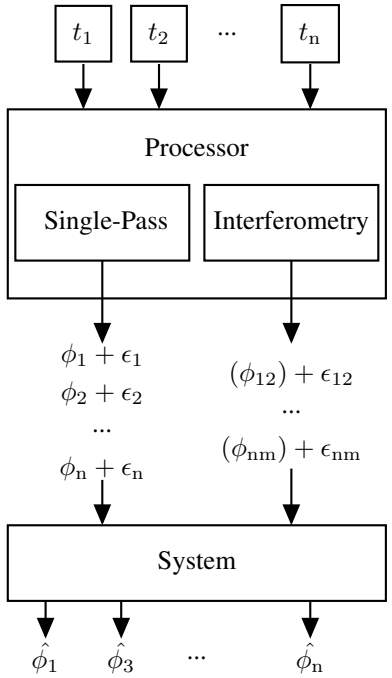

Figure 1 Block diagram for data combination.

Figure 1 shows the block diagram of the scheme that we propose for the updated estimation of the ionospheric phase errors. First, the image stacks for all available times,

t_1 to t_n, must be processed separately in a single pass calibration step. For this paper, we consider the case in which an MDA is applied, but in a more refined approach, a combination with the Faraday rotation can also be used. The output would be a first set of estimations of the absolute phases (ϕ_1, ϕ_2 to ϕ_n) with the associated errors (ϵ_1, ϵ_2 to ϵ_n) that are determined by the performance of the calibration algorithms.

At the same time, interferometric combinations of all possible pairs are used to estimate the interferometric phase screen that corresponds to the differential ionosphere, ϕ_{nm}, again with the errors ϵ_{nm} that correspond to the performance of the calibration algorithm. More sensitivity and resolution are expected in the interferometric calibration but will only produce differential phase variations.

Finally, all this information is fed into a Least Squares (LS) system that makes the single-pass estimations compatible with the interferometric estimations. Under the assumption that calibration errors (ϵ_1, ϵ_2 to ϵ_n) are independent of each other, an LS tries to cancel them out, leading to single-pass solutions with improved resolution ($\hat{\phi}_1$, $\hat{\phi}_2$ to $\hat{\phi}_n$). An LS system was chosen because it has proven to integrate different estimations when (as in this case) the data combination can be expressed as a set of linear operations. A system for a stack of three images is shown in (1).

$$\underbrace{\begin{bmatrix} 1 & 0 & 0 \\ 0 & 1 & 0 \\ 0 & 0 & 1 \\ 1 & -1 & 0 \\ 1 & 0 & -1 \\ 0 & 1 & -1 \end{bmatrix}}_{\text{LT}} \underbrace{\begin{bmatrix} \hat{\phi}_1 \\ \hat{\phi}_2 \\ \hat{\phi}_3 \end{bmatrix}}_{\text{combined estimation}} = \underbrace{\begin{bmatrix} \phi_1 + \epsilon_1 \\ \phi_2 + \epsilon_2 \\ \phi_3 + \epsilon_3 \\ \phi_{12} + \epsilon_{12} \\ \phi_{13} + \epsilon_{13} \\ \phi_{23} + \epsilon_{23} \end{bmatrix}}_{\text{calibration output}} \quad (1)$$

As inputs to the system, there are all phases recovered from the MDA in this case ($\phi_n + \epsilon_n$) and all the differential phases extracted from interferometric methods [10] ($\phi_{nm} + \epsilon_{nm}$). The system is over-determined since the number of unknowns is just the number of images in the stack, and the number of equations is the stack length plus the number of interferometric pairs. It will be shown that adding weights to the system can make the solution more robust.

3 Simulation Scenario

Due to the lack of Biomass data, for this work, it was decided to inject simulated 1D ionospheric phase errors into a TerraSAR-X reflectivity image (Figure 2) by partially focusing at the height of maximum ionization, h_{iono} [6]. To the detected reflectivity, partially correlated realizations of multiplicative speckles were added (simulating temporal decorrelation). This was done up to seven times since it is the number of passes defined for Biomass' tomographic phase.

The spatial distribution of the ionospheric irregularities, responsible for quickly changing phase errors, which are smaller than the outer scale l_0 (that range starting from $\sim$ 5 km [12], well below the synthetic aperture length) is described by a power law spectrum [13]

$$\Phi_\phi(\kappa) = \frac{\lambda^2 \cdot r_e \cdot \sec^2\theta \cdot ab \cdot (2\pi/1000)^{p+1} \cdot C_k L}{(\kappa_0^2 + \kappa^2)^{(p+1)/2}}, \quad (2)$$

where κ is the spatial wave number, λ is the wavelength that corresponds to the carrier frequency f_0, r_e is the classical electron radius, θ is the incidence angle onto the ionosphere, ab is the anisotropy ratio, p is the spectral index, $C_k L$ is the vertically integrated turbulent strength at 1km scale and $k_0 = 2\pi/l_0$ is the outer scale wave number.

For this study, we are also focusing on the single-pass calibration case where only the MDA was applied. Running the experiments over an actual reflectivity image is necessary to assess the performance of the MDA in retrieving the quickly varying ionospheric irregularities. The simulation parameters are summarized in Table 1.

Parameter	Units	Value
Wavelength λ	m	0.69
Incidence angle θ	deg	25
Anisotropy $a:b$	-	5:1
Spectral index p	-	2.65
Turbulent strength $C_k L$	-	10^{33}
Outer scale l_0	km	20
Satellite height h_{sat}	km	660
Ionospheric height h_{iono}	km	350

Table 1 Simulation parameters.

4 Results

In this results section, we are going to focus on two main points: first, we will focus on the output of the ionospheric recovery with the MDA for one case, then the discussion can be extrapolated to all other cases; second, we will show the results obtained from the combination framework.

4.1 Single-Pass Solution

The MDA performance is affected by (i) the block-wise operation, (ii) the limited resolution in the estimation of second derivatives due to the averaging of the synthetic aperture, and (iii) the limitation of the bounding the random walks errors in the integration. The block operation also produces a down-sampled estimate of the phase error that we up-sample again with a linear interpolation. With all this, the single-pass inconsistencies are made of aliasing, low-pass filtering, and interpolation errors.

Figure 3 shows the profiles of the recovered phase after five iterations, and one can see the limitation of retrieving very fast varying phases. Another way to see it is in Figure 4, which shows the interferometric phase error contribution from the ionosphere between the images before and after applying MDA with respect to the same image with no ionosphere for one of the scenarios. This is what we will refer to as single-pass solutions. Note that after applying

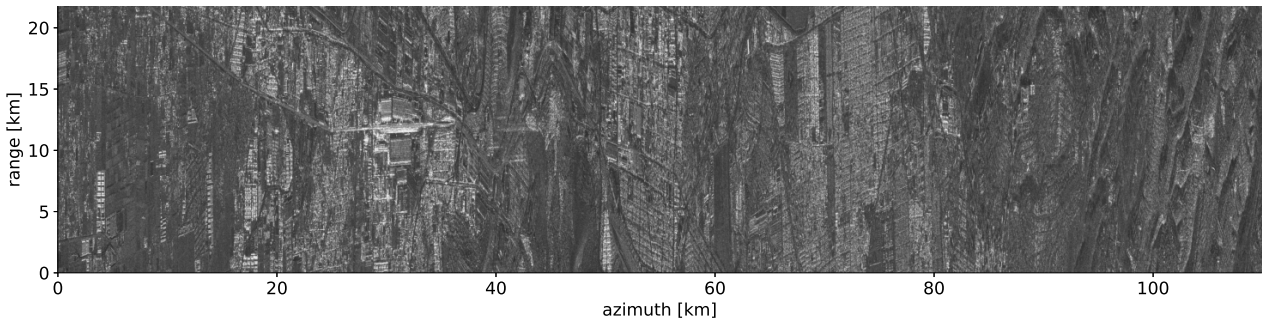

Figure 2 Reflectivity of TerraSAR-X image over Mexico used in the simulations.

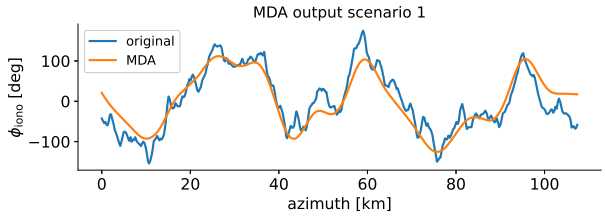

Figure 3 Recovered phase profile with MDA.

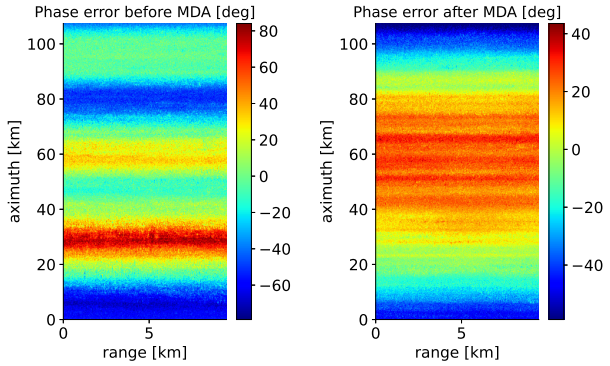

(a) Phase error before applying MDA. **(b)** Phase error after applying MDA.

Figure 4 Interferometric phase with respect to the image with no ionosphere for one of the scenarios. Note the different color scales.

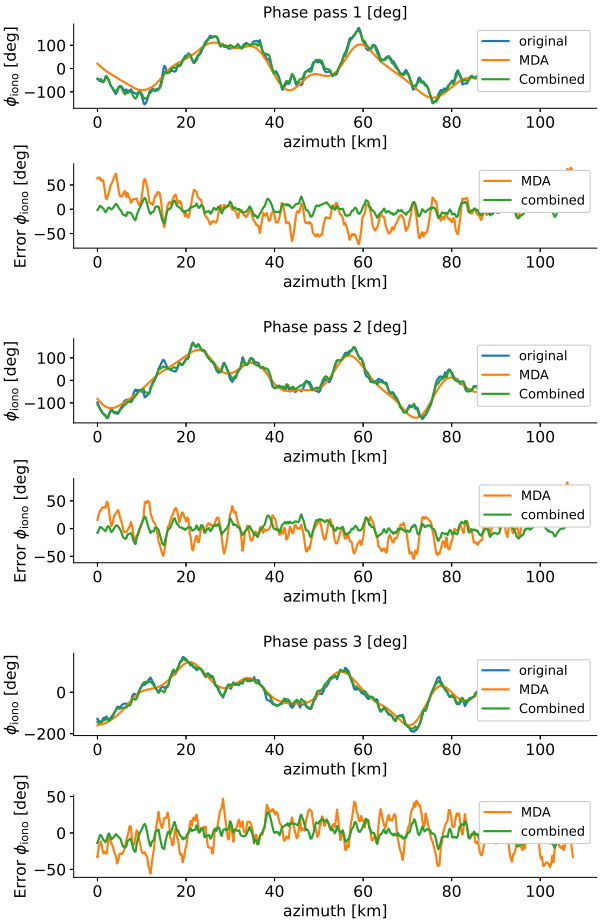

Figure 5 Phase profiles recovered by combining the information of seven different passes with the single pass solutions.

the MDA, there is a high-frequency phase component left behind that will not only contaminate the interferometric product but also leave residual defocusing.

4.2 Combined solution

As an example for the simulation of seven passes, Figure 5 compares three of the single-pass phases obtained with the MDA only separately in each image, with the combined solution after combining with the interferometry of all possible pairs. Note that in the error curves, it is possible to see how residual trends are canceled out and the magnitude of the errors is reduced, which translates into a gain in resolution.

Figure 6 shows the root mean square (RMS) residual error for all ionospheric phases as a function of the stack length. If the errors are uncorrelated, in principle, the more information put in the estimator, the better. In this case, this is not what is seen after five passes. The performance of the MDA depends on the structure of the phase error itself, and in the fifth image ϵ_5 was remarkably larger. The system in (1) can be extended to a Weighted Least Squares (WLS) to compensate for this (here case using the covariance of the error). Figure 7 shows the result of using a weighted system.

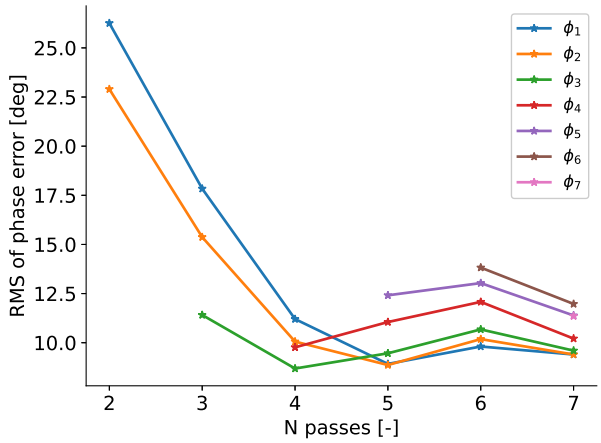

Figure 6 RMS of error with number of passes that are being used for the estimation.

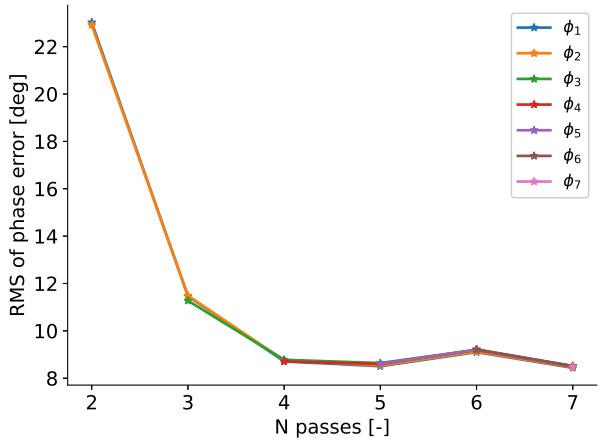

Figure 7 RMS of error with number of passes that are being used for the estimation in a weighted system.

Finally, after obtaining the new ionospheric estimation ($\hat{\phi}_1$, $\hat{\phi}_2$ to $\hat{\phi}_n$), they can be fed back into the calibration chain to obtain single images with even smaller phase errors. Figure 8 shows a histogram of the residual phase in the image before and after applying the MDA (the map in Figure 4) and after correcting with the phase recovered in the top panel in Figure 5.

5 Conclusions

The ionospheric calibration of Biomass products has two steps: first, at a single image level, and later, an interferometric calibration. The interferometric calibration provides high sensitivities but of the differential ionosphere only. On the other hand, ionospheric imaging and calibration with single images are limited by the performance of the calibration algorithm (in this paper we focused on the MDA). We presented a method that can be used to gain resolution in the absolute ionospheric realizations through a Least-Squares filter that cancels out inconsistencies in the

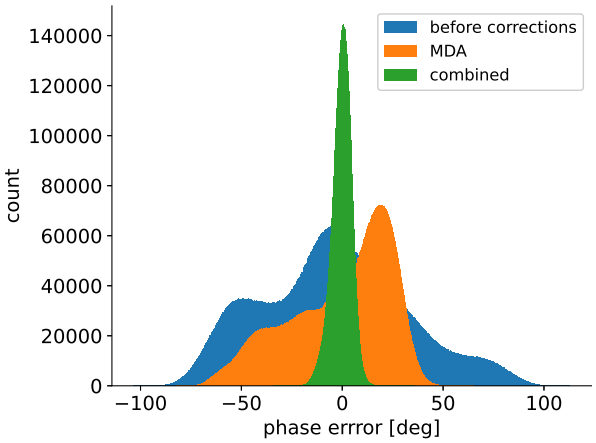

Figure 8 Histograms of interferometric phase errors with respect of the image without ionosphere.

single-pass products by utilizing what is measured in the interferometric calibration step.

By injecting different simulated phase errors into a reflectivity image with the Biomass's parameters, it was possible to test that this approach can cancel residual trends in the estimation of the phase errors compared to the MDA solution and that higher-frequency errors could be resolved. It was also shown that the RMS of the solution decreases with the number of images available to input into the system.

This framework can be extended to add other effects in the processing, like errors in the interferograms due to noise and decorrelation. It can also be adapted to separate the dispersive ionospheric component to the interferogram from other geophysical signals (such as the motion of surfaces and topography) by adding more equations (from other measurements if available) to keep the system determined.

6 Literature

[1] "Report for mission selection: Biomass," Tech. Rep. (ESA SP-13214/1), European Space Agency (ESA), Noordwijk, The Netherlands, November 2012.

[2] F. J. Meyer and J. Nicoll, "The impact of the ionosphere on interferometric sar processing," in *IGARSS 2008-2008 IEEE International Geoscience and Remote Sensing Symposium*, vol. 2, pp. II–391, IEEE, 2008.

[3] Z.-W. Xu, J. Wu, and Z.-S. Wu, "A survey of ionospheric effects on space-based radar," *Waves in Random media*, vol. 14, no. 2, p. S189, 2004.

[4] F. Meyer, R. Bamler, N. Jakowski, and T. Fritz, "The potential of low-frequency sar systems for mapping ionospheric tec distributions," *IEEE Geoscience and Remote Sensing Letters*, vol. 3, no. 4, pp. 560–564, 2006.

[5] D. Belcher, "Theoretical limits on sar imposed by the

ionosphere," *IET Radar, Sonar & Navigation*, vol. 2, no. 6, pp. 435–448, 2008.

[6] J. S. Kim, K. P. Papathanassiou, R. Scheiber, and S. Quegan, "Correcting distortion of polarimetric sar data induced by ionospheric scintillation," *IEEE Transactions on Geoscience and Remote Sensing*, vol. 53, no. 12, pp. 6319–6335, 2015.

[7] C. V. Jakowatz, D. E. Wahl, P. H. Eichel, D. C. Ghiglia, and P. A. Thompson, *Spotlight-mode synthetic aperture radar: a signal processing approach: a signal processing approach*. Springer Science & Business Media, 2012.

[8] F. Betancourt-Payan, M. Rodriguez-Cassola, A. Benedikter, P. Prats-Iraola, and G. Krieger, "An autofocus algorithm for the recovery of ionospheric phase signatures in the biomass mission," in *EUSAR 2022; 14th European Conference on Synthetic Aperture Radar*, pp. 1–5, VDE, 2022.

[9] V. Gracheva, J. S. Kim, P. Prats-Iraola, R. Scheiber, and M. Rodriguez-Cassola, "Combined estimation of ionospheric effects in sar images exploiting faraday rotation and autofocus," *IEEE Geoscience and Remote Sensing Letters*, vol. 19, pp. 1–5, 2021.

[10] G. Gomba and F. De Zan, "Bayesian data combination for the estimation of ionospheric effects in sar interferograms," *IEEE Transactions on Geoscience and Remote Sensing*, vol. 55, no. 11, pp. 6582–6593, 2017.

[11] S. Tebaldini, A. M. Guarnieri, and F. Rocca, "Recovering time and space varying phase screens through sar multi-squint differential interferometry," in *EUSAR 2012; 9th European Conference on Synthetic Aperture Radar*, pp. 16–19, VDE, 2012.

[12] J. Aarons, "Global morphology of ionospheric scintillations," *Proceedings of the IEEE*, vol. 70, no. 4, pp. 360–378, 1982.

[13] D. Belcher and N. Rogers, "Theory and simulation of ionospheric effects on synthetic aperture radar," *IET radar, sonar & navigation*, vol. 3, no. 5, pp. 541–551, 2009.